ORIGINAL RESEARCH PAPER

Heat flux estimation from borehole temperatures acquired during logging while tripping: a case study with the sea floor drill rig MARUM-MeBo

T. Freudenthal[1] · H. Villinger[2] · M. Riedel[3] · T. Pape[1,2]

Abstract

During trip out of the drill string at the end of a drilling operation (logging while tripping) borehole temperatures can be measured without the need for additional operational time. A simple interpretation of the measured borehole temperatures is difficult due to the interfering influences of the drilling operations, mainly due to flushing the borehole during drilling. In this study, we present borehole temperature data from drilling campaigns with the sea floor drill rig MARUM-MeBo200 at the Danube Deep Sea Fan (Black Sea) and west of Taiwan (South China Sea). The temperature measurements were conducted with a PT1000 temperature sensor which is integrated in a memory acoustic borehole logging tool. We developed a modeling approach in order to simulate the drilling perturbations and subsequent evolution of the temperature field within the borehole. By fitting the model data to the measured time dependent temperature depth profiles, we estimated the undisturbed heat flux at the drill sites. This study shows that knowledge of the pattern of drilling operations with alternating phases of drilling/flushing and drill string handling is crucial for comparing temperatures measured during logging while tripping and simulated temperatures.

Keywords MeBo sea floor drill rig · Borehole logging · Borehole temperature · Geothermal heat flux

Introduction

The thermal structure of the subsurface is an important parameter for characterizing diagenetic conditions and processes at depth, the deep biosphere habitat, rheologic conditions or the stability field of gas hydrates (Wilson et al. 2001; Searle and Escartín 2004; Villinger et al. 2010; Becker et al. 2020; Heuer et al. 2020; Riedel et al. 2021). Formation temperatures determined in boreholes in combination with formation thermal conductivity allow estimation of heat flux which is key for predicting the thermal structure of the subsurface beyond the drilling depth (Prensky 1992). The drilling process affects temperature measurements in boreholes during and immediately after drilling, mainly by flushing. Therefore, either measurements have to be conducted with a delay after drilling (days to months) until the drilling disturbance has disappeared and the temperatures inside the borehole reflect true formation temperatures. Or correction methods like the Horner-plot method based on repeated temperature logs after mud circulation ceased should be used (Goldberg 1997; Henninges et al. 2005; Inagaki et al. 2013).

Since most non-commercial and uncased offshore wells collapse after some time, repeated temperature measurements are not possible. Therefore, in the context of scientific offshore drilling, a method was developed starting in the 1980s, in which a temperature sensor is pushed into unconsolidated or semi-consolidated sediments at the bottom of the borehole (for details of history of temperature measurements in scientific ocean drilling boreholes see Heesemann et al. 2006 and references therein). When a sensor is pushed into the sediment at the base of the borehole, frictional heat is generated that requires some waiting time for dissipation

✉ T. Freudenthal
freuden@marum.de

1 MARUM—Center for Marine Environmental Sciences, University Bremen, Leobener Str. 8, 28359 Bremen, Germany

2 Faculty of Geosciences, University of Bremen, Klagenfurter Str. 2–4, 28334 Bremen, Germany

3 GEOMAR Helmholtz Centre for Ocean Research Kiel, Wischhofstrasse 1–3, 24148 Kiel, Germany

and/or model-based correction (Heesemann et al. 2006; Villinger et al. 2010).

A push-in temperature probe similar to the one used by the International Ocean Discovery Program (Davis et al. 1997) was developed for the use with robotic sea floor drill rigs like the MARUM-MeBo (Freudenthal and Wefer 2013; Kopf et al. 2013). This probe contains a miniature temperature logger (MTL; Pfender and Villinger 2002). However, measurements with the MTL push-in probe require additional operational time (about 1 h per discrete measurement in case of the use with MeBo) and reduce core quality at the intervals analyzed for temperatures. The MTL push-in probe is thus mainly used when the investigation of the temperature gradient is a major goal of the scientific objectives of the expedition (e.g., Riedel et al. 2018, 2020b, 2021).

Autonomous slim-hole memory logging tools are used for open-hole borehole logging with the MeBo (Freudenthal and Wefer 2013). The tool is inserted into the drill string once the target drilling depth is reached. During trip out, the tool is pulled up together with the lowermost section of the drill string and protrudes out of the drill bit into the open hole. In this way, logging of physical properties of the uncased formation is possible. The so-called logging while tripping method does not require extra time since the drill string has to be tripped out anyway (Freudenthal and Wefer 2013; Kück et al. 2021). It additionally allows borehole logging in unstable formations since the drill string stabilizes the upper portion of the borehole (Matheson and West 2000). Several different logging tools exist for the use with MeBo measuring spectral gamma ray, electric conductivity and magnetic susceptibility. The most recent development is a memory acoustic tool (MAT, Fig. 1) specifically designed for the use with MeBo. This tool is equipped with one acoustic transmitter and two receivers for measuring p-wave velocities of the formation. In addition, a temperature sensor is integrated for measuring the fluid temperature within the borehole.

During research expedition M142 the drill rig MARUM-MeBo200 was used to recover sediment cores from the Danube deep sea fan in the Black Sea for various analyses

(Bohrmann et al. 2018; Pape et al. 2020 ; Riedel et al. 2020a) and for measurements of formation temperature profiles (Riedel et al. 2021). Measurements of (i) formation temperature with the MTL push-in probe and (ii) borehole fluid temperature with the MAT were conducted within the same borehole down to a drilling depth exceeding 140 m below sea floor (mbsf). Comparison of the two temperature data sets revealed a striking similarity of both profiles (Fig. 2) despite the impact of flushing during drilling. This similarity encouraged us to investigate, if borehole temperatures
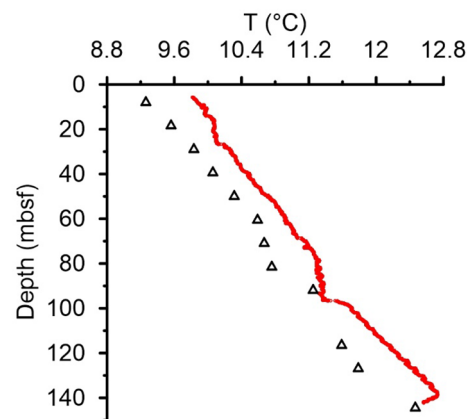
Fig. 2 Formation temperature data determined with the MTL push-in probe (Riedel et al. 2021; black open triangles) and borehole temperature data (red dots) measured as upcast during trip out with the temperature sensor of the MAT at site DDSF (GeoB22605; modified from Bohrmann et al. 2018). Formation temperatures were each collected at the base of the borehole while interrupting the process of downward drilling. They are compensated for the impact of cooling by flush water (Riedel et al. 2021). Borehole temperature measurements started approximately 75 min after having reached the maximum drill depth and flushing was stopped. Note that the temperature sensors of the MTL push-in probe and the MAT are designed for different temperature ranges (-5 to $+60$ °C and -20 to $+80$ °C, respectively). As a consequence, the accuracy of the two methods (0.1 K and 1 K, respectively) differ such that only trends but no absolute temperature values can be evaluated together
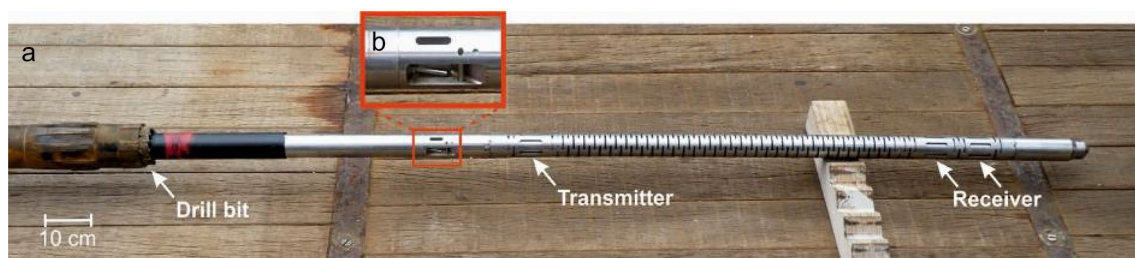
Fig. 1 **a** Memory Acoustic Tool (MAT) with transmitter and two receivers developed for logging while tripping with the sea floor drill rig MARUM-MeBo. The sensor part fits through the drill bit (lowest part of the drill string) while the logger part is attached inside of the drill string to the shoulder of the drill bit. The red box marks the position of the temperature sensor for measuring borehole temperatures, that is shown enlarged in **b**

measured with the MAT during trip out can be used to infer undisturbed formation temperatures and estimate heat flux.

In this study we analyze borehole temperature data collected with MeBo during two research expeditions, SO266 in the South China Sea in 2018 (Bohrmann et al. 2019) and M142 in the Black Sea in 2017 (Bohrmann et al. 2018). We present a new method for estimating geothermal heat flux based on borehole temperature measurements acquired in the logging while tripping mode. Our strategy is to use a forward model and grid search in which we simulate the drilling and trip out processes and compare simulated temperatures with those measured during trip out. The main purpose of this investigation is to explore if the temperatures measured during tripping out contain useful information for the estimation of heat flux. As a sort of feasibility study, we used a modeling approach, which is comparatively simple in order to assess the scientific potential of the information contained in the measured temperatures. Our approach is by no means an in-depth-modeling study but should be regarded as a first step.

Study sites and methods

Drill sites

We used the sea floor drill rig MeBo200 (Freudenthal and Wefer 2013) at four sites (Table 1) for drilling up to 144 mbsf in order to recover sediments and to conduct borehole logging. Abbreviations and variables used in this manuscript are listed in the supplementary informations (Tab. S1 and Tab. S2, respectively). During research expedition M142 (Bohrmann et al. 2018), borehole temperature logging was conducted at drill site GeoB22605, which was located on a levee complex adjacent to a channel at the Danube Deep Sea Fan (DDSF; supplementary informations Fig. S1) mainly built up by fine-grained marine and lacustrine sediments.

Two ridges with active gas seeping close to the drill sites were drilled and logged during research expedition SO266 (Bohrmann et al. 2019) in the South China Sea (supplementary informations Fig. S2). Site GeoB23213 located on the southern summit of the Formosa Ridge (SSFMR) is an erosional structure at the passive continental margin of the Eurasian plate. Four-Way Closure Ridge is an accretionary ridge at the subduction zone southwest of Taiwan with sites GeoB23231 (FWCR-S) and GeoB23234 (FWCR-N) located on the southern and northern part of Four-Way Closure Ridge, respectively. The drilled formations at both ridges consist mainly of hemipelagic muds. Evidence for the presence of gas hydrates were found at site FWCR-S below about 65 mbsf and at site SSFMR below 94 mbsf (Bohrmann et al. 2019).

Drilling and borehole logging

The drill rig MeBo200 is deployed on the sea floor and remotely controlled from the research vessel. We used wire-line core drilling tools with a stroke length of 3.5 m. The drill bit outer diameter was 103 mm. Ambient bottom sea water was used for flushing until the target drill depth was reached. Freudenthal and Wefer (2013) describe in detail the wire-line rotary drilling operation with the MeBo.

Borehole logging data were acquired with a combined tool string of a spectrum gamma ray tool and the MAT, developed by ANTARES Datasystems GmbH (www.antares-geo.de). Here, we focus on the temperature data collected by the MAT with an integrated platinum resistance sensor (PT1000) for the measurement of borehole fluid temperature (Fig. 1). The temperature measuring range is − 20 to + 80 °C, the absolute accuracy within the limits of the measuring range is about 1 K. The resolution of the temperature measurements is about 0.003 K. The borehole logging tool string with 44 mm diameter was connected to a memory adapter with 70 mm diameter that contains batteries

Table 1 Overview on MeBo drill sites considered in this study. Since only borehole logging was conducted at site GeoB23231-1 but no cores were taken, sediment porosity measurements for cores taken from Site GeoB23216-1 in the same area are considered

Site	Area	Short code	Latitude (N)	Longitude (E)	Water depth (m)	Drilling depth (mbsf)	References
GeoB22605-1	Black Sea, Danube deep sea fan	DDSF	43° 55.95′	30° 49.75′	765	144.0	Bohrmann et al. (2018)
GeoB23213-1	South China Sea, Southern Summit Formosa Ridge	SSFMR	22° 06.89′	119° 17.14′	1134	109.0	Bohrmann et al. (2019)
GeoB23231-1 (GeoB23216-1)	South China Sea, Four-Way Closure Ridge South	FWCR-S	22° 02.92′	119° 48.09′	1318	143.9 (126.5)	Bohrmann et al. (2019)
GeoB23234-1	South China Sea, Four-Way Closure Ridge North	FWCR-N	22° 03.46′	119° 48.05′	1348	59.9	Bohrmann et al. (2019)

as energy source and a data logger for storing the measured borehole data. The memory adapter contains an internal clock that was synchronized with GPS-time (UTC) when programming the logging tools. The sampling rate was 0.5 Hz.

Borehole logging with the tool string was conducted in the logging while tripping mode: Once the target drilling depth is reached and the last inner core barrel is recovered, trip out is started by lifting the drill string by ~ 3.5 m and disconnecting the upper rod. Before continuing with the trip out, the borehole logging tool string is dropped into the drill string. The landing shoulder of the borehole logging tool string lands on the drill bit with the logging tools having passed the drill bit and sticking out in the open borehole between bottom of the borehole and drill bit. The tool string is hooked up inside the borehole by tripping out the drill string (logging while tripping). The trip out speed is usually set at about 0.01 m s^{-1} and interrupted for about 5–20 min each 3.5 m (stationary phases) for disconnecting the upper rod of the drill string before trip out is continued. Temperatures measured during these stationary phases are the basis of the comparisons between observations and simulation.

No flush water was pumped into the borehole during the entire trip out process. Within this study, the first and only borehole logging was conducted with the described MAT tool string at each reported site. For the used tool string arrangement, the temperature sensor was located about 1.8 m (at drill site DDSF) and 1.0 m (at drill sites SSFMR, FWCR-S, FWCR-N) below the drill bit, respectively. The distance to the base of the borehole during start of the trip out was 1.8 and 2.6 m, respectively. The distance of the drill bit to the base plate of the drill rig (defined as position of the sea floor: 0 mbsf) was recorded by the depth control system of the MeBo. The accuracy of the depth measurement of the drill bit position below the base plate of the drill rig is about 0.1% of the drill depth. GPS-time (UTC) was used as reference for the depth measurement.

Modeling

We used the FlexPDE® finite element software package (www.pdesolutions.com) to model the temperature evolution within the borehole during drilling and logging. The geometry of the model is that of a cylinder with an axial-symmetry with the borehole being located at the axial center of the cylinder. The radius of the cylinder is 10 times the diameter of the drill string and the length of the cylinder is 3 times the maximum borehole depth. The vertical coordinate is scaled by the maximum length of the cylinder (i.e., 3 times the maximum borehole depth) to facilitate discretization of the model with finite elements. For numerical stability reasons the model assumes that the drill string is already in place (supplementary informations Fig. S3) before drilling starts. Since the thermal conductivity of the drill string is about two orders of magnitude greater than that of the formation and the wall thickness is small compared to the borehole diameter, the temperature profile within the borehole before drilling begins corresponds to the temperature profile in the formation.

The drill string has an outer diameter of 95 mm and a wall thickness of 7.5 mm. The thread connectors used for coupling the rods consist of steel (42CrMo4) and contribute 10% to the total length of the drill string. To simplify the model, we assumed a weighted mix of the physical properties of aluminum (90%) and steel (10%). No annulus is assumed, i.e. the borehole diameter is equal to the drill string outer diameter. Table 2 summarizes the material parameters of formation, borehole and drill string.

The boundary conditions are as follows: (1) before drilling starts, the temperature profile within the cylinder is determined by the preset constant heat flux Q at the bottom

Table 2 Diameters of borehole (n.a.: not applicable) and drill string as well as material characteristics of borehole, drill string, and formation. The depth range that is characterized by uniform lithology and that was therefore used for estimating thermal conductivity and for comparing model results with measurements is given in brackets. Specific thermal conductivities were used for the different formations at individual sites according to sediment porosity values. Thermal diffusivity was calculated as ratio of thermal conductivity to the product of density and specific heat capacity

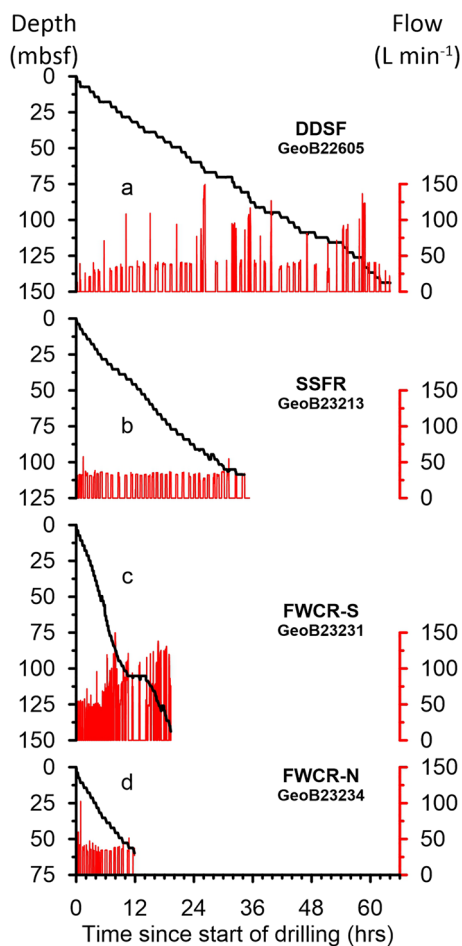|	Outer/Inner Diameter (mm)	Density (kg m^{-3})	Specific heat capacity (J K^{-1} kg^{-1})	Thermal conductivity (W m^{-1} K^{-1})	Thermal diffusivity (10^{-7} m^2 s^{-1})
Borehole	n.a./103	1024	4000	0.6	1.46
Drill string	95/80	3166	857	103.26	381
Formation					
DDSF (0–79 m)		1600	2400	1.4	3.64
SSFMR (0–78 m)		1600	2400	1.28	3.33
FWCR-S (0–68 m)		1600	2400	1.25	3.26
FWCR-N (0–40 m)		1600	2400	1.24	3.23

Fig. 3 Drill depth (black) and flush sea water flow rate (red) for all four drill sites investigated in this study

of the cylinder and the assumed constant thermal conductivity of the formation; (2) without limitation of generality of the results, the temperature at the surface (z = 0) is set to zero for all times; (3) heat flux at the circumferential surface area of the cylinder is set to zero which means that the isotherms are perpendicular to the circumferential surface area, which prevents any horizontal heat flux loss.

The complete process of drilling and logging is simulated by solving the time-dependent heat conduction equation. Drilling is simulated as follows: in the center of the cylinder the thermal conductivity structure is changed with time (and hence depth), depending on the alternation of drilling and adding a new pipe-segment based on the recorded drilling history (see Fig. 3 and Figure S3 of supplementary informations). During drilling phases, water is continuously flushed within the borehole and flushing is simulated using an extremely high thermal conductivity value (i.e., 1000 W K^{-1} m^{-1}) resulting in almost isothermal temperature within the borehole. During the 5–20 min

long stationary phases (phases with no depth change; see Fig. 3), thermal conductivity of the borehole is set back to the conductivity of water (Table 2) and core barrels are exchanged and drill rods are added to the drill string. During all times, water inside the borehole exchanges heat conductively with the formation.

FlexPDE® creates the finite element grid (supplementary informations Fig. S4) automatically and refines it during the modeling process if errors are larger than a preset value (0.001 K). The number of cells is on the order of several thousand. Time steps are also iteratively adjusted by FlexPDE® starting with values less than one second but increase during the complete modeling run. Runtime for a single model run depends on the complete drilling-operation time. In case of borehole DDSF the runtime is about 15 min on a desktop computer for the longest drilling duration of about 2.7 days.

Observations (supplementary informations Fig. S5) show that the water inside the drill string is not isothermal just before logging while tripping starts. This means that the water column is warmed up by the formation and warming increases with the continuation of drilling when the borehole reaches in deeper and warmer formations along the geothermal gradient. We simulated this in the model by assuming a linear increase of water temperature with drilling-time up to a maximum temperature T_{max} when the final drill depth is reached.

For each model run, we assume a basal heat flux and a value of T_{max}. After each run, we determine the modeled temperatures during the stationary phases while logging (see Figs. 4 and 5) and compare the modeled with the observed temperatures as well as the adaption rates.

For this comparison, model temperatures were shifted by the estimated bottom water temperature determined by linear extrapolation of the uppermost three borehole temperature measurements to the sediment water interface (see Table S3 of supplementary informations). These estimates agree very well with bottom water temperature measurements by CTD cast at all for sites (Bohrmann et al. 2018; Mau and Bohrmann 2020).

No direct measurements of thermal conductivities exist for this study. The thermal conductivity of the formation $k_{formation}$ within the investigated intervals (Table 2) is assumed to be constant and is derived from average fractional porosity φ measured on samples of the recovered core using an empirical relationship:

$$k_{formation} = k_{fluid}^{\phi} \, k_{matrix}^{1-\phi}$$

with $k_{fluid} = 0.6$ W K^{-1} m^{-1} and $k_{matrix} = 3.0$ W K^{-1} m^{-1} (Brigaud and Vasseur 1989; Goto and Matsubayashi 2008).

Riedel et al. (2020a) published porosity values of site DDSF. Porosity measurements at sites SSFMR, FWCR-S,
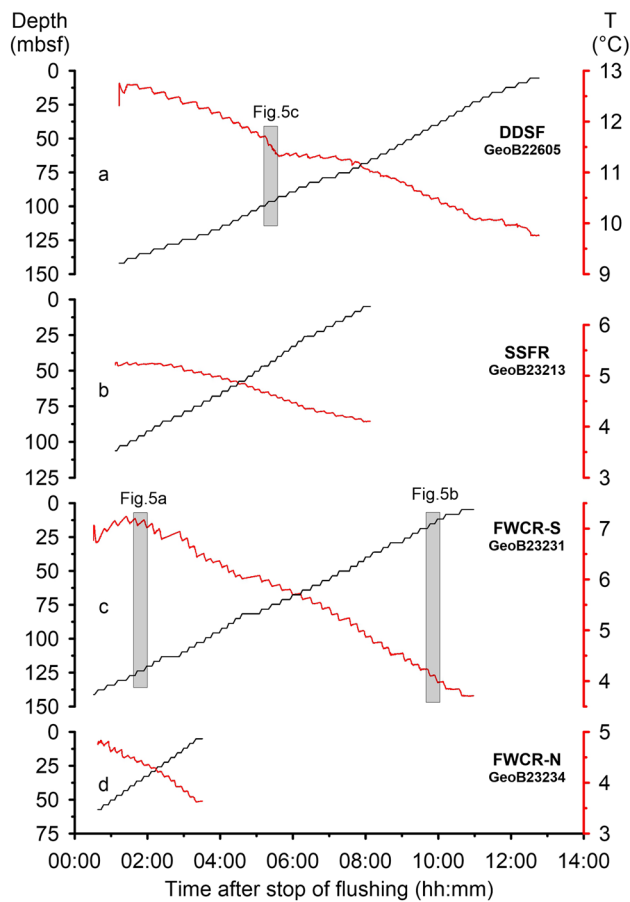
Fig. 4 Logged temperature (red) and sensor depth (black) during trip out at all four drill sites investigated in this study. Time is recorded starting with the end of drilling operation as soon as the last flushing was stopped. Data within the grey boxes are shown in detail in Fig. 5a–c

Fig. 5 Three examples for temperature measurements during phases of trip out of the drill string and constant depth (stationary phase; depth: black solid line; temperature: red dots). Shown are blowups of grey boxes marked in Fig. 4. Temperature adaption rates dT/dt are calculated as linear fit of temperature vs. time (solid blue line) during stationary phases. Average temperatures T_{av} are arithmetic means of temperature measurements during the stationary phases

and FWCR-N are presented in the supplementary informations (Fig. S6). For the calculation of a constant $k_{formation}$, we averaged porosities of the upper section of the borehole (Table 2), which are characterized by uniform lithology (Bohrmann et al. 2018, 2019) and constant porosity.

Results

Drilling operation

An overview on the drilling operation for all four sites considered is presented in Fig. 3 and in Table 3. The operational procedure took longest at the Black Sea Site DDSF with more than 2.5 days, when coring was interrupted for a number of in-situ formation temperature measurements (Riedel et al. 2021). Drilling progress was fastest at site FWCR-S, where the maximum drill depth of 144 mbsf was reached within less than 1 day. Apart from two pressure core barrel
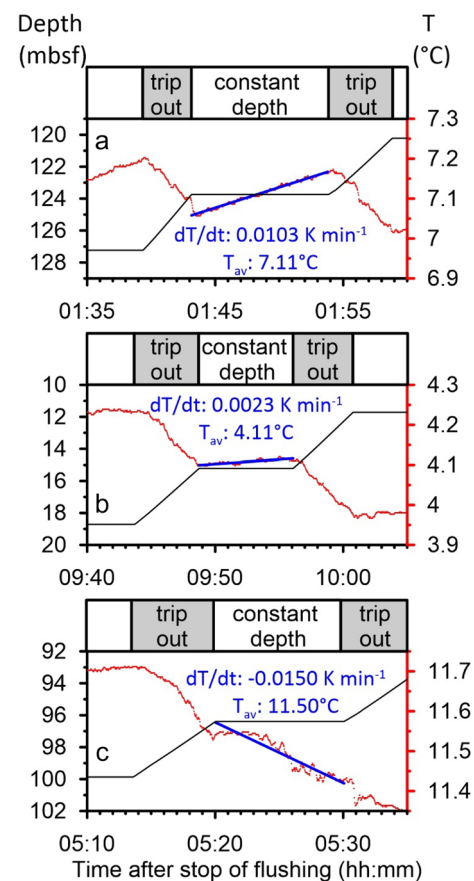
deployments (see Pape et al. 2017, for a technical description) at around 105 mbsf, no cores were taken during this deployment. Almost half of the operational time at this site was related to drilling time with sea water being pumped into the borehole. Flush rates were higher with about 74 L min^{-1} compared to 31–45 L min^{-1} at the other three sites (Table 3).

Measured borehole temperatures

An overview on borehole temperatures measured during trip out of the drill string for all four sites is presented in Fig. 4. A stepwise decrease in temperature corresponds to a stepwise decrease of depth at which the sensor was located in the borehole. The stepwise profiles reflect alternating periods of trip out and periods of constant depth (Fig. 5). Periods of constant depth (stationary phases) lasted on average about 10 min, which corresponds to the time required

Table 3 Statistics of drilling operations. Total borehole volume excluding the drill string volume was calculated based on drill depth and drill string dimensions given in Table 1 and Table 2

Site	Start of drilling operation	End of drilling operation	Start of logging	Duration	Drilling/ flushing time	Average flush volume	Total borehole volume
		(dd.mm.yy hh:mm UTC)		(h)	(h)	(L min^{-1})	(L)
DDSF	16.11.17 14:32	19.11.17 06:28	19.11.17 07:44	63.93	15.22	44.5	287
SSFMR	22.10.18 15:02	24.10.18 01:19	24.10.18 02:31	34.28	13.3	31.5	218
FWCR-S	8.11.18 11:49	9.11.18 07:05	9.11.18 07:38	19.27	8.25	74.3	287
FWCR-N	10.11.18 14:32	11.11.18 02:28	11.11.18 03:07	11.93	5.15	36.1	120

for unscrewing the upper 3.5 m long drill rod from the drill string and its storage in the MeBo magazine before continuing with the trip out of the next 3.5 m stroke.

In most cases, an increase in temperature occured during the stationary phases. This clearly indicates that adaption of borehole temperatures to formation temperature (steady state undisturbed temperature before drilling was started) was an ongoing process during the entire period of measurements. Relatively high temperature adaptation rates (dT/dt) were particularly observed within the stationary phases at the beginning of the borehole logging (i.e., within the deeper portion of the boreholes). During such phases, temperatures rose close to the starting temperature of the previous trip out phase (Fig. 5a). For measurements at shallow borehole depths, when several hours have already passed since the stop of flushing with bottom sea water, the temperature adaption rates during stationary phases were lower (Fig. 5b). Temperature data from all South China Sea drill sites (SSFMR, FWCR-S, and FWCR-N) showed a similar pattern of temperature adaption rates during the stationary phases (Fig. 6): Highest rates of up to 0.0365 K min^{-1} were observed during the beginning of the measurements. Rates gradually decreased within the first two hours after stop of drilling operations. After the first two hours, temperature adaption rates remained low at about 0.0014 ± 0.0005 K min^{-1} (SSFMR), 0.0029 ± 0.0017 K min^{-1} (FWCR-S), and 0.0015 ± 0.0007 K min^{-1} (FWCR-N), respectively. In a few cases, a drop of temperature occurred during a stationary phase (Fig. 5c; Fig. 6a–c). Remarkably, phases of strong temperature drop with temperature adaption rates up to -0.0268 K min^{-1} only occurred at the Black Sea site DDSF (Fig. 7b).

Averaged borehole temperatures at all sites showed an increase with depth during the stationary phases (T_{av}, Fig. 7a). Exceptions were observed for the deepest part where temperature disturbance was most severe as the time between stop of flushing and measurement was short (less than 2 hours). At the Black Sea Site DDSF, a local temperature minimum was determined in the deepest part of
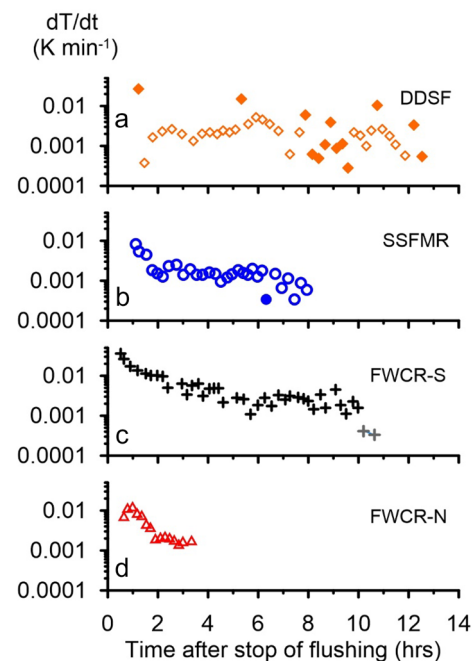
Fig. 6 Temperature adaption rates dT/dt (logarithmic scale) for **a** the Black Sea site DDSF (GeoB22605) and **b**–**d** the South China Sea sites SSFMR (GeoB23213), FWCR-S (GeoB23231), and FWCR-N (GeoB23234). Rates were calculated as linear fit of temperature vs. time during stationary phases as indicated in Fig. 5. Solid or grey markers indicate negative temperature adaption rates (temperature decreases with time during stationary phase). At site FWCR-N **d**, a relatively low rate of 3×10^{-5} K min^{-1} 3 hours and 10 minutes after stop of flushing is out of the scale range and not presented here

the borehole at 141.9 mbsf, although indicated by a single data point only. A second local temperature minimum was present at around 93 mbsf. Both minima at this site were accompanied by negative temperature adaption rates (Fig. 7b).

Differences in the temperature gradients between the four investigated sites (Fig. 7c) are likely indicative for the variability of the regional heat flux, although the signal was overprinted by the ongoing temperature adaption. Measurements in the upper parts of the borehole were characterized by

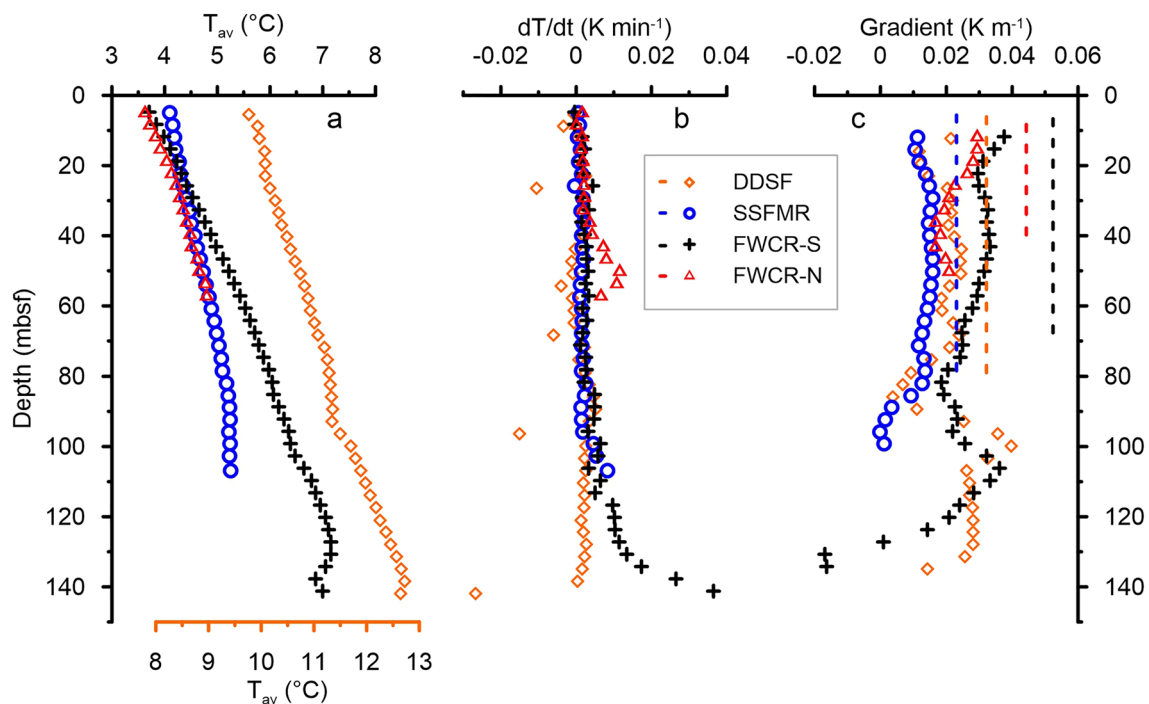**Fig. 7 a** Average temperatures T_{av}, **b** temperature adaption rates dT/dt, and **c** temperature gradients vs. borehole depth for all four drill sites investigated. Average temperatures and temperature adaption rates were calculated for phases of constant depth as indicated in Fig. 5. Average temperatures for the Black Sea drill site DDSF (GeoB22605) relate to the orange bottom axis, while those for the South China Sea drill sites SSFMR (GeoB23213), FWCR-S (GeoB23231), and FWCR-N (GeoB23234) relate to black top axis. Temperature gradients **c** within the boreholes were calculated by linear regression using a sliding window of 5 adjacent measurements (17.5 m). Dashed lines indicate the modeled formation temperature gradients at the four sites

low temperature adaption rates of less than 0.003 K min⁻¹. The largest temperature gradients within the borehole of about 0.030 K m⁻¹ on average were found at sites FWCR-S (upper 60 m of the borehole) and FWCR-N (upper 22 m). At sites SSFMR and DDSF average temperature gradients in the upper 60 m were lower with 0.014 K m⁻¹ and with 0.020 K m⁻¹, respectively.

Modeled temperatures

The drilling history at all four drill sites is well constrained and was used for modeling the temperature evolution within the borehole during and after drilling. Only the upper sections of the borehole were considered for fitting measured and modeled temperatures as these sections were characterized by uniform lithology and porosity, which conforms to our assumption of constant thermal conductivity of the formation (Table 2). The modeled temperature evolution depends on the assumed basal heat flux Q in the area as well as on the maximal warming of the flush sea water T_{max} within the borehole. We computed 545 models in total with different heat flux and T_{max} values (Fig. 8) in order to find the best fit of simulated and measured temperatures within the borehole. Figure 8 shows contours of the average

temperature difference avδT between model and measurement during the stationary phases. The contour of avδT = 0 represents a perfect fit of simulated and measured temperatures for a given combination of T_{max} and Q. At all four sites, a linear relationship between selected T_{max} and Q was observed for those model runs with avδT = 0 (Fig. 8). If modeled temperature adaption rates (dT/dt$_{model}$) are less than zero, the model is marked by red filled circles, otherwise by blue circles.

In the strategy for selecting the best representative model, we used the following criteria: (1) avδT = 0, and (2) dT/dt$_{model}$ ≥ 0. A third criterion is a minimal difference $δT_0$ between modeled temperature at the deepest location of the MAT temperature sensor and measured temperatures T_0 just before tripping out. The reason for criterion (1) is obvious—we want a minimal difference between modeled and measured temperatures. Criterion (2) is based on the fact that we observed in most cases (except for DDSF) temperature adaption rates above or close to zero. Criterion (3) answers the question, if the modelled temperature at the bottom of the hole at the end of the drilling phase is in good agreement with the measured temperature just before the start of the tripping out phase. Figure 9 shows the selection of the best fit using all three criteria.
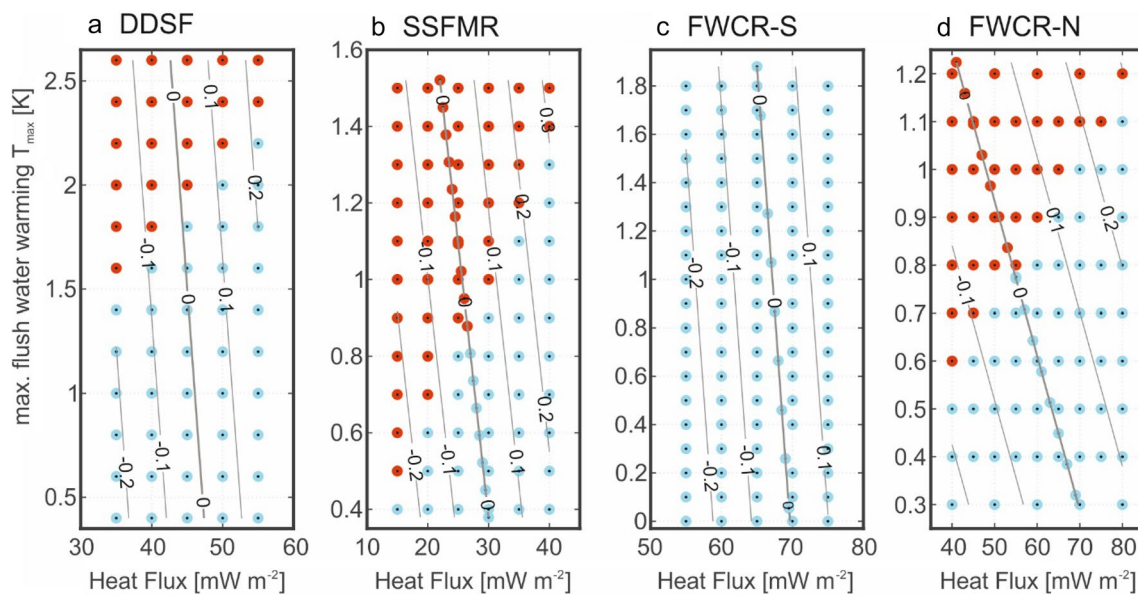
Fig. 8 Result of search for optimal fit of modeled and measured borehole temperature data at the four drill sites **a–d** in dependence of chosen maximal warming of flush sea water (T_{max}) and basal heat flux. Contour lines show the interpolated avδT values (difference between modeled and measured borehole temperatures averaged for the upper section of the borehole with uniform lithology) with avδT$=0$ being the first criterium for choosing the optimal model. Blue dots mark simulations that correspond to the second criterium based on the modeled temperature adaption rate with dT/dt$_{model} \geq 0$

As an example, the comparison of modeled and measured temperature data for the optimal fit at site FWCR-S is shown in Fig. 10a. The modeled borehole temperature before start of the trip out generally increases with depth. However, below 19 mbsf it is lower than the assumed initial formation temperature. The modeled temperatures for the stationary phases match very well with the measured temperatures in the depth interval between 5 and 68 mbsf, the zone of assumed constant thermal conductivity. This is also indicated by differences between modeled and measured temperatures δT of less than 0.1 K (Fig. 10b). δT values increase below 68 mbsf to amounts close to 0.4 K. However, the overall pattern with a local maximum in borehole temperature at about 130 mbsf is reproduced well by the modeled temperatures. Higher temperature adaption rates in the lowest part of the borehole below 110 mbsf are also reproduced by the model (Fig. 10c), although modeled temperatures in the upper part of the borehole above 110 mbsf are generally lower than measured.

The parameters identified for the best fit at all four sites are summarized in Table 4. The uncertainty of the modeled temperatures expressed by the average deviation of the modeled and measured temperatures within the zone of assumed constant thermal conductivity expressed as root mean square (RMS) value is less than 0.06 K. For the South China Sea sites, the modeled temperature adaption rates generally fit the observed patterns (Fig. 11a), although especially low rates < 0.01 K min^{-1} are frequently underestimated by the

model (Fig. 11b). However, the model failed to reproduce the negative excursion of temperature adaption rates for the Black Sea site DDSF (Fig. 11a). Modeled geothermal fluxes at site SSFMR located on Formosa Ridge at the passive continental margin are 29.5 mW m^{-2} and lower than those at sites FWCR-S and FWCR-N on Four-Way Closure Ridge at the active continental margin (65.5 and 55 mW m^{-2}, respectively). The best fit at site DDSF was achieved with a geothermal flux of 45 mW m^{-2}. Modeled formation temperature gradients for undisturbed conditions (Table 4) at all four sites are higher compared to the corresponding gradients calculated by linear regression of the measured borehole temperatures T_{av} (Fig. 7).

Discussion

This study is the first attempt in using temperature data from the MAT to estimate heat flux. We succeeded in reproducing the observed borehole temperature depth profiles with an uncertainty of less than or equal to 0.06 K at all four drill sites investigated. This is remarkable, since the model is based on several strong simplifications like a constant thermal conductivity and the simplified modeling of the drilling process. Potential turbulence within the borehole resulting from drop-in of the logging tool and from trip out of the drill string are neglected by the model as well as transport of heat by trip out of the drill string and the tool string.
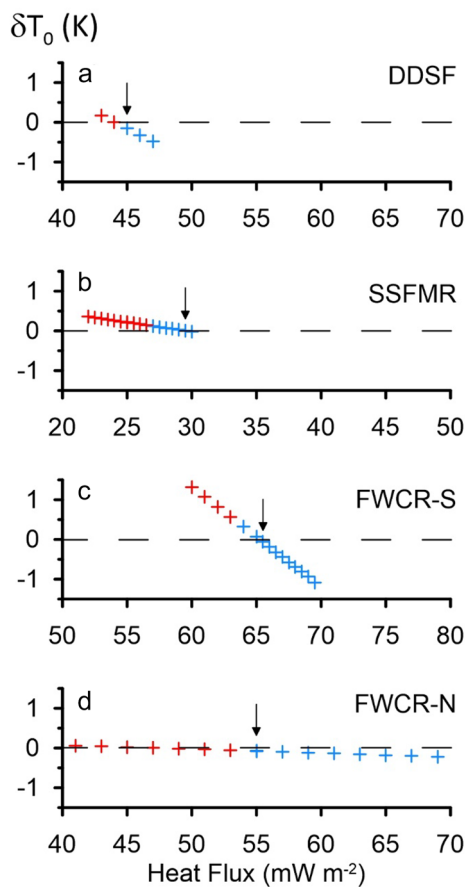
δT_0 (K)

Fig. 9 Difference between modeled and measured borehole temperature during start of the measurement δT_0 at the four drill sites **a**–**d** plotted against basal heat flux Q. Only model runs that fulfil the first selection criterium $av\delta T = 0$ are considered. Blue crosses mark simulations that correspond to the second criterium based on the modeled temperature adaption rate with $dT/dt_{model} \geq 0$. Arrows mark the selected model run according to the third criteria with δT_0 being close to zero

In addition, we lack crucial information like the temperature profile within the borehole just before start of the tripping out procedure. The uncertainty of the fit is in general larger than temperature variability during stationary phases resulting from the ongoing temperature adaption during the measurement but in a lot of cases only by a factor of two to three. Therefore, temperature adaption rates provide a very good quality control of the model simulation although the stationary phases varied significantly in duration (5–25 min). As stationary phases are fairly short due to operational time constraints, extrapolating measured temperature during this period to undisturbed formation temperature is not feasible.

Highest temperature adaption rates were measured and modeled at the bottom of the borehole. This is reasonable, since both the temperature difference between flush water and formation temperature is highest and the time for temperature recovery is shortest. However, flush water warms

up during the way to the bottom of the hole. On the return line back to the surface warmed-up flush water may cause a temperature increase during drilling operation in the upper sediments. This is also the case for the simplified model where a flush water temperature profile constant with depth within the borehole during drilling operation is applied. Warming of the flush water is described by a linear increase of flush water temperature with progress of drilling up to a value T_{max}. However, at least for the South China Sea sites SSFR, FWCR-N and FWCR-S positive temperature adaption rates indicate a net cooling during drilling operation. We conclude, that cooling by the introduction of the drill string with much higher thermal conductivity compared to the sediments overcompensates a potential warming by warmed-up flush water especially in the upper sediments.

In contrast, the measured profile at the Black Sea site DDSF shows several zones with negative temperature adaption rates. Borehole temperature measurements at this site were affected by the active formation of gas hydrates within the borehole during drilling. Here, logging was conducted after drilling through the gas hydrate stability zone (GHSZ) into a formation that contained free gas at the base of the borehole (Riedel et al. 2021). Gas bubbles escaped the borehole during the entire logging process and the temperature probe was covered by gas hydrates when recovered from the borehole. Gas bubbles and ascending gas hydrates probably caused additional turbulent water flow within the borehole. Therefore, the formation of gas hydrates and turbulent mixing in the borehole are the most likely causes, why the model failed to reproduce the measured irregular depth pattern of temperature adaption rates (Fig. 6a). Since the formation of gas hydrate is an exothermic process, it is reasonable that the modeled geothermal gradient of 0.0322 K m^{-1} was considerably higher than the 0.0238 $\pm$ 0.02 K m^{-1} estimated from in-situ formation temperature measurements at the same site (Riedel et al. 2021).

The modeled geothermal fluxes at the South China Sea sites were lowest at site SSFMR on the crest of Formosa Ridge. This is reasonable, considering the tectonic setting of this area and strong topographic effects on the near-surface temperature field. Formosa Ridge is located at the passive continental margin while the other two sites FWCR-S and FWCR-N on the crest Four-Way Closure Ridge are located within a subduction-collision system (Teng 1990). Based on the depth of the GHSZ, Chen et al. (2014) estimated the temperature gradient at Formosa ridge to be ~0.037 K m^{-1}. This is considerably higher than the 0.0231 K m^{-1} established in our study. However, both, topographic effects and fluid flow, have an impact on the interpretation of the geothermal field from the depth of the GHSZ (Chen et al. 2014). A similar approach was conducted for the area of Four-Way Closure Ridge by Kunath et al. (2020), who estimated background temperature gradients ranging from 0.028 to 0.039 K m^{-1}
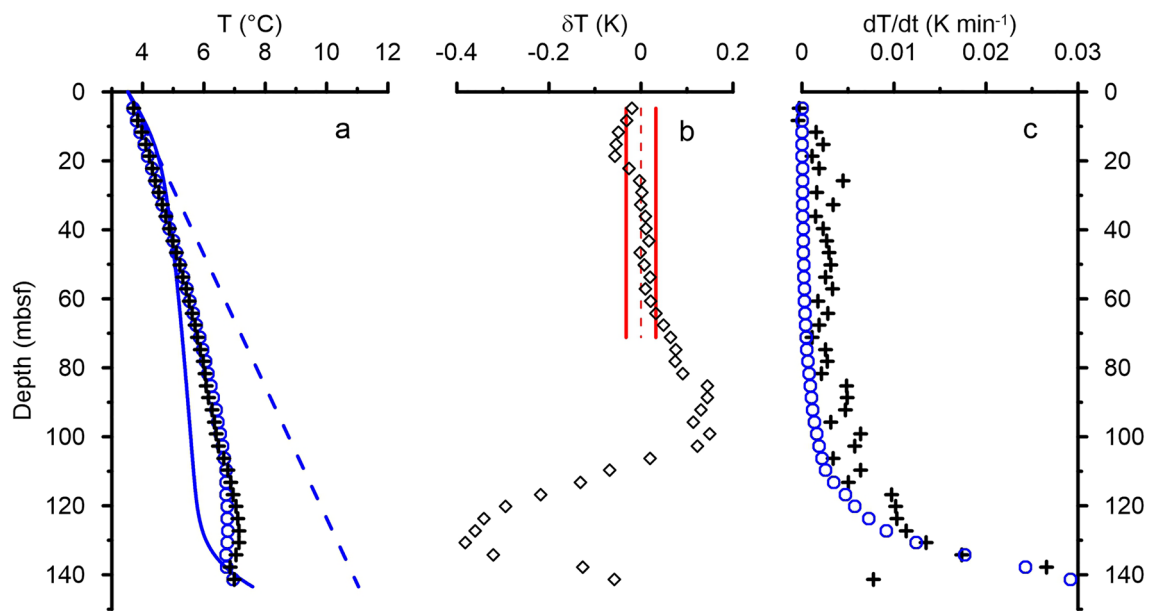
Fig. 10 Modeling results at site FWCR-S for the optimal fit with $T_{max} = 1.678$ K and heat flux $= 65.5$ mW m^{-2}. **a** Modeled borehole temperatures before start of trip out (blue solid line), assumed initial formation temperature (blue dashed line), and modeled temperatures (blue circles) at the same depth and time compared to measured average temperatures at phases of constant depth (black crosses); **b** Dif-ference between modeled and measured temperatures at phases of constant depth (black diamonds). Red dashed and solid lines mark average ± 1 standard deviation (-0.010 K± 0.026 K) for the depth interval of assumed constant thermal conductivity, between 5 and 78 mbsf. **c** Modeled (blue open circles) and measured (black crosses) temperature adaption rates at phases of constant depth

based on the depths of the GHSZ. Local shoaling of the GHSZ in the vicinity of faults were explained by fluid migration and geothermal gradients as high as 0.052 K m^{-1} (Kunath et al. 2020). These gradients are supported by measurements with a 6-m long heat flow probe (Kunath et al. 2020). Remarkably, the results of our study are in the upper range of the reported gradients which is reasonable, considering that both drill sites FWCR-S and FWCR-N were located close to active seep sites (Bohrmann et al. 2019).

Knowledge of the thermal conductivity profile is essential for a reliable estimation of heat flux based on comparing modeled and measured borehole temperatures. In this study, we estimated average thermal conductivities by using porosity measurements on core samples collected on

board. Estimated thermal conductivities at sites FWCR-S and FWCR-N are similar to published values in that area (Kunath et al. 2020). In future MeBo drilling projects measurements of thermal conductivity on cores (minimum of two at each end of the core) are needed to characterize the thermal conductivity profile. Since porosities are also measured on core samples, these thermal conductivity spot measurements can in turn be used for calibrating the empirical relationship between porosity and thermal conductivity.

An adequate characterization of the impact of drilling perturbations, in particular (i) cooling of the borehole wall and the formation in the vicinity of the borehole by flushing and (ii) the effect of the drill string with a thermal conductivity three magnitudes higher than formation values, is crucial for modelling the temperature evolution with time inside the borehole. In this study, we simplified the impact of flushing with sea water by (1) an extremely high thermal conductivity of the drilling fluid during drilling phases and (2) by introducing the T_{max} value that describes an assumed warming of flush water down to the base of the borehole. Despite this simplification, good agreement between modeled and measured borehole temperatures as well as temperature adaption rates was achieved.

One important constraint for the quality control of the model is the temperature profile right after the drilling phase ends and just before the tripping out (and logging) phase starts (see supplementary informations Fig. S5). This profile

Table 4 Summary of optimal fit model parameters T_{max} (parameter describing the warming of flush water within the borehole) and Q (basal heat flux). RMS defines the root mean square of the difference between modeled and measured data within the interval of assumed constant thermal conductivity

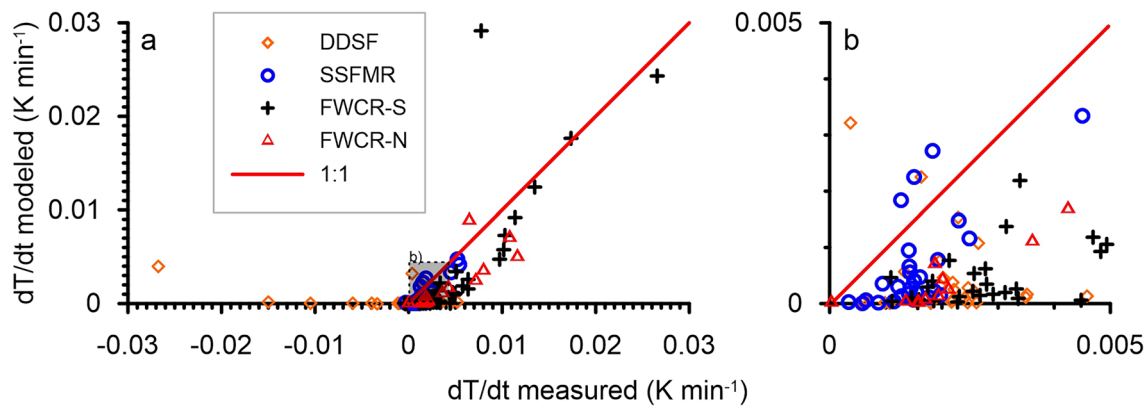| Site	RMS (K)	T_{max} (K)	Q (mW m^{-2})	Formation temperature gradient (K m^{-1})
DDSF	0.0404	1.50	45.0	0.0322
SSFMR	0.0583	0.45	29.5	0.0231
FWCR-S	0.0315	1.68	65.5	0.0524
FWCR-N	0.0089	0.77	55.0	0.0443

Fig. 11 a Comparison of measured and modeled temperature adaption rates for all four sites. The red line marks the 1:1 relationship that would be expected for a perfect fit. Data within the grey box are shown in detail in **b**

is measured during the descent of the logging tool until it lands on the drill bit. Unfortunately, there is no depth control of the temperature probe while it sinks. Therefore, measured temperatures cannot be used to reconstruct the temperature profile, as the sinking velocity is not known in detail. We recently added a pressure sensor to the logging tool to overcome this issue. Therefore, in future applications it will be possible to have depth control of the temperature readings especially while the probe sinks to the lower end of the drill string. In addition, it could be helpful to monitor temperatures of sea water at the suction line of the flush water line as well as in the vicinity of the borehole outflow in order to check the model assumptions. For future applications, we also recommend to increase the times of constant depth to at least 10 min each during tripping out. This would allow a more systematic and better estimation of temperature adaption rates especially at the end of the experiment when adaption rates are low.

Since the model only considers conductive heat exchange processes between formation and borehole, low formation permeability and no fluid/heat advection is a prerequisite for the application of the method proposed herein. Penetration of cold flush water into the formation e.g., in sands or highly fractured rocks would potentially increase the formation cooling impact by the drilling operation. Zones with high permeability may be conduits for lateral fluid flow with the potential of disturbing the temperature profile within the borehole. On the other hand, temperature anomalies within boreholes could be used to infer on lithologic changes indicating strata with higher permeability.

This study shows that useful information on lithology and temperature field can be gained by carefully evaluating borehole temperatures measured during trip out in combination with data of the drilling history. Borehole temperatures can be measured with a borehole logging tool during trip out of the drill string without additional time requirement.

Data sets used in this study were optained from gas-hydrate focused drilling projects and the four boreholes were drilled into complex gas-hydrate bearing lithologies. In addition, all boreholes are located in areas with strong variations in seabed relief. It would be desirable to test our new method during future MeBo drilling projects in settings, where there is as little seafloor topography as possible, where lithology is fairly uniform and where co-located seafloor heat flux measurements would help to establish confidence in our presented approach.

Conclusions

Borehole temperature measurements can be easily conducted and combined with additional geophysical borehole logging during trip out of the drill string (logging while tripping) at the end of a drilling operation. Especially temperature data collected during stationary phases, that occur in regular intervals during disconnecting drill rods from the drill string, allow the estimation of borehole temperature as function of depth and time. The combined analysis of the temperature profile and temperature adaption rates also enables detection of lithologic changes. By modelling the temperature evolution with time within the borehole, it is possible to estimate the regional heat flux. The model proposed in this study includes information on the drilling history in order to simulate the impact of drilling perturbation on the local temperature field. We believe that this method is suitable for the analysis of any borehole temperature data collected after the drilling operation (logging while tripping). A reliable determination of formation thermal conductivity is key for the interpretation of the borehole temperature data. Further investigations, especially comparison of model-derived formation temperatures with direct measurements, are needed to validate geothermal heat fluxes derived from borehole

temperatures measured during logging while tripping. For a consistent validation of the method, a new experiment should be conducted within an environment with smooth topography, with a lack of fluid mobilization, outside the gas hydrate stability zone, and with homogeneous cohesive sediments with little variations in thermal conductivity as possible.

Supplementary Information The online version contains supplementary material available at https://doi.org/10.1007/s11001-022-09500-1.

Declarations

Conflicts of interest We have no conflict of interest to declare.

References

Becker K, Davis EE, Heesemann M, Collins JA, McGuire JJ (2020) A long-term geothermal observatory across subseafloor gas hydrates, IODP hole U1364A, Cascadia accretionary prism. Front Earth Sci. https://doi.org/10.3389/feart.2020.568566

Bohrmann G, Ahrlich F, Bachmann K, Bergenthal M, Beims M, Betzler C, Brünjes J, Deusner C, Domeyer B, Düßmann R, Ewert J, Gaide S, Frank C, Freudenthal T, Fröhlich S, Greindl T, Haeckel M, Heitmann-Bacza C, Ion G, Kaszemeik K, Keil H, Kinski O, Klein T, Kossel E, Linowski E, Malnati J, Mau S, Meyer B, Pape T, Popa A, Renken J, Reuter J, Reuter M, Riedel M, Riemer P, Rohleder C, Rosiak U, Rotaru SG, Rothenwänder T, Stachowski A, Seiter C, Schmidt W, Utecht C, Vasilev A, Wallmann K, Wegwerth A, Wintersteller P and Wunsch D (2018) R/V METEOR cruise report M142, Drilling Gas Hydrates in the Danube Deep-Sea Fan, Black Sea, Varna—Varna—Varna, 04 November—22 November—09 December 2017, Berichte, MARUM—Zentrum für Marine Umweltwissenschaften, Fachbereich Geowissenschaften, Universität Bremen, 320:1–121 http://nbn-resolving.de/urn:nbn:de:gbv:46-00106617-14

Bohrmann G, Ahrlich F, Bergenthal M, Berndt C, Chen J, Chen S, Chen T, Chen W, Chi W, Deusner C, Elger J, Freudenthal T, Fröhlich S, Klein T, Kramer L, Kuhnert M, Fan L, Hsu H, Lai M, Lin S, Lin T, Mai H, Mau S, Malnati J, Meyer-Schack B, Niederbockstrut B, Pape T, Rosiak U, Stachowski A, Stamp A, Tseng Y, Tu T, Wallmann K, Wang Y, Wetzel G, Wei K, Wintersteller P, Wu Y, Wunsch D, Yu P (2019) R/V SONNE cruise report SO266/1, MeBo200 Methane Hydrate Drillings Southwest of Taiwan, TaiDrill, Cruise No. 266/1, 15 October—18 November 2018, Kaohsiung (Taiwan)—Kaohsiung (Taiwan). SONNE-Berichte; SO266/1; 1–201. doi: https://doi.org/10.48433/cr_so266_1

Brigaud F, Vasseur G (1989) Mineralogy, porosity and fluid control on thermal conductivity of sedimentary rocks. Geophys J 98:525–542. https://doi.org/10.1111/j.1365-246X.1989.tb02287.x

Chen L, Chi W-C, Wu S-K, Liu C-S, Shyu C-T, Wang Y, Lu C-Y (2014) Two dimensional fluid flow models at two gas hydrate sites offshore southwestern Taiwan. J Asian Earth Sci 92:245–253. https://doi.org/10.1016/j.jseaes.2014.01.004

Davis EE, Villinger H, MacDonald RD, Meldrum RD, Grigel J (1997) A robust rapid-response probe for measuring bottom-hole temperatures in deep-ocean boreholes. Mar Geophys Res 19:267–281. https://doi.org/10.1023/A:1004292930361

Freudenthal T, Wefer G (2013) Drilling cores on the sea floor with the remote-controlled sea floor drill rig MeBo. Geosci Instr Methods Data Sys 2(2):329–337. https://doi.org/10.5194/gi-2-329-2013

Goldberg D (1997) The role of downhole measurements in marine geology and geophysics. Rev Geophys 35:315–342. https://doi.org/10.1029/97RG00221

Goto S, Matsubayashi O (2008) Inversion of needle-probe data for sediment thermal properties of the eastern flank of Juan de Fuca

Ridge. J Geophys Res 113:B08105. https://doi.org/10.1029/2007JB005119

Heesemann M, Villinger H, Fisher AT, Tréhu AM, White S (2006) Data report: testing and development of the new APC3 tool to determine in situ temperatures while piston coring. In Riedel, M., Collett, T.S., Malone, M.J., and the Expedition 311 Scientists, Proc. IODP, 311: Washington, DC (Integrated Ocean Drilling Program Management International, Inc.). doi:https://doi.org/10.2204/iodp.proc.311.108.2006

Henninges J, Schrötter J, Erbas K, Huenges E (2005) Temperature field of the Mallik gas hydrate occurrence—implications on phase changes and thermal properties. In: Dallimore SR, Collett TS (eds) Scientific results from the Mallik 2002 Gas hydrate research production research well program. Geological Survey of Canada, Ottawa, p 14

Heuer VB, Inagaki F, Morono Y, Kubo Y, Spivack AJ, Viehweger B, Treude T, Beulig F, Schubotz F, Tonai S, Bowden SA, Cramm M, Henkel S, Hirose T, Homola K, Hoshino T, Ijiri A, Imachi H, Kamiya N, Kaneko M, Lagostina L, Manners H, McClelland HL, Metcalfe K, Okutsu N, Pan D, Raudsepp MJ, Sauvage J, Tsang MY, Wang DT, Whitaker E, Yamamoto Y, Yang K, Maeda L, Adhikari RR, Glombitza C, Hamada Y, Kallmeyer J, Wendt J, Wörmer L, Yamada Y, Kinoshita M, Hinrichs KU (2020) Temperature limits to deep subseafloor life in the Nankai Trough subduction zone. Science 370(6521):1230–1234. https://doi.org/10.1126/science.abd7934

Inagaki F, Hinrichs K-U, Kubo Y., Expedition 337 Scientists (2013) Proceedings of the Integrated Ocean Drilling Program. Doi:https://doi.org/10.2204/iodp.proc.337.103.2013

Kopf A, Asshoff K, Belke-Brea M, Bergenthal M, Bohrmann G, Bräunig A, Düssmann R, Feseker T, Fleischmann T, Franke PD, Geprägs P, Hammerschmidt S, Heesemann B, Herschelmann O, Hüpers A, Ikari MJ, Kaszemaik KM, Kaul N, Kimura T, Kitada K, Klar S, Lange M, Madison M, Mai AH, Noorlander C, Pape T, Rehage R, Reuter C, Reuter M, Rosiak UD, Saffer DM, Schmidt W, Seiter C, Spiesecke U, Stachowski A, Takanori O, Tryon M, Vahlenkamp M, Wei J, Wiemer G, Wintersteller P, Zarrouk MK (2013). Report and preliminary results of R/V SONNE cruise SO222. MEMO: MeBo drilling and in situ Long-term Monitoring in the Nankai Trough accretionary complex, Japan. Leg A: Hong Kong, PR China, 09.06.2012—Nagoya, Japan, 30.06.2012. Leg B: Nagoya, Japan, 04.07.2012—Pusan, Korea, 18.07.2012. Berichte, MARUM—Zentrum für Marine Umweltwissenschaften, Fachbereich Geowissenschaften, Universität Bremen, No. 297, 121 pp, Bremen, 2013. urn:nbn:de:gbv:46-00103543-13

Kück J, Groh M, Töpfer M, Jurczyk A, Harms U (2021) New geophysical memory-logging system for highly unstable and inclined scientific exploration drilling. Sci Dril 29:39–48. https://doi.org/10.5194/sd-29-39-2021

Kunath P, Chi W-C, Berndt C, Chen L, Liu C-S, Kläschen D, Muff S (2020) A shallow sea bed dynamic gas hydrate system off SW Taiwan: results from 3-D seismic, thermal, and fluid migration analyses. J Geophys Res: Sol Earth. https://doi.org/10.1029/2019JB019245

Matheson R, West J (2000) Logging while tripping—a new alternative in formation evaluation. J Can Petrol Technol 39:38–43. https://doi.org/10.2118/00-07-02

Mau S, Bohrmann G (2020) Physical oceanography at CTD stations of Sonne cruise SO266. PANGAEA. https://doi.org/10.1594/PANGAEA.915954

Pape T, Hohnberg H-J, Wunsch D, Anders E, Freudenthal T, Huhn K, Bohrmann G (2017) Design and deployment of autoclave pressure vessels for the portable deep-sea drill rig MeBo (Meeresboden-Bohrgerät). Sci Drill 23:29–37. https://doi.org/10.5194/sd-23-29-2017

Pape T, Haeckel M, Riedel M, Kölling M, Schmidt M, Wallmann K, Bohrmann G (2020) Formation pathways of light hydrocarbons in deep sediments of the Danube deep-sea fan, Western Black Sea. Mar Pet Geol 122:104627. https://doi.org/10.1016/j.marpetgeo.2020.104627

Pfender M, Villinger H (2002) Miniaturized data loggers for deep sea sediment temperature gradient measurements. Mar Geol 186:557–570. https://doi.org/10.1016/S0025-3227(02)00213-X

Prensky S (1992) Temperature measurements in boreholes—an overview of engineering and scientific applications. Log Anal 33(3):313–333

Riedel M, Wallmann K, Berndt C, Pape T, Freudenthal T, Bergenthal M, Bünz S, Bohrmann G (2018) In situ temperature measurements at the Svalbard Continental Margin: implications for gas hydrate dynamics. Geoch Geophys Geosys 19:1165–1177. https://doi.org/10.1002/2017GC007288

Riedel M, Freudenthal T, Bergenthal M, Haeckel M, Wallmann K, Spangenberg E, Bialas J, Bohrmann G (2020a) Physical properties and core-log seismic integration from drilling at the Danube deep-sea fan. Black Sea Marine Pet Geol 114:104192. https://doi.org/10.1016/j.marpetgeo.2019.104192

Riedel M, Villinger H, Freudenthal T, Pape T, Bünz S, Bohrmann G (2020) Thermal characterization of pockmarks across Vestnesa and Salvator Ridges offshore Svalbard. J Geophys Res Solid Earth. https://doi.org/10.1029/2020JB019468

Riedel M, Freudenthal T, Bialas J, Papenberg C, Haeckel M, Bergenthal M, Pape T, Bohrmann G (2021) In-situ borehole temperature measurements confirm dynamics of the gas hydrate stability zone at the upper Danube deep sea fan, Black Sea. Earth Plan Sci Let. https://doi.org/10.1016/j.epsl.2021.116869

Searle RC, Escartín J (2004) The rheology and morphology of oceanic lithosphere and mid-ocean ridges. In: German CR, Lin J, Parson LM (eds) Mid ocean ridges: hydrothermal interactions between the lithosphere and the oceans. American Geophysical Union, Washington, D.C., pp 63–93

Teng LS (1990) Geotectonic evolution of late Cenozoic arc-continent collision in Taiwan. Tectonophysics 183(1–4):57–76. https://doi.org/10.1016/0040-1951(90)90188-E

Villinger HW, Tréhu AM, Grevemeyer I (2010) Seafloor marine heat flux measurements and estimation of heat flux from seismic observations of bottom simulating reflectors. Geohysical characterization of gas hydrates. Society of Exploration Geophysicists, Houston, pp 279–300

Wilson AM, Sanford WE, Whitaker FF, Smart P (2001) Spatial patterns of diagenesis during geothermal circulation in carbonate platforms. Am J Sci 301(8):727–752. https://doi.org/10.2475/ajs.301.8.727